

Published in final edited form as:

*Proteins*. 2016 April ; 84(4): 532–543. doi:10.1002/prot.24999.

# Computational Analysis of the CB1 Carboxyl-terminus in the Receptor-G Protein Complex

**Joong-Youn Shim**[1,*], **Leepakshi Khurana**[2], and **Debra A. Kendall**[2]

[1]Department of Chemistry, University of North Carolina, Chapel Hill, NC 27514

[2]Department of Pharmaceutical Sciences, University of Connecticut, Storrs, CT 06269-3092

## Abstract

Despite the important role of the carboxyl-terminus (Ct) of the activated brain cannabinoid receptor one (CB1) in the regulation of G protein signaling, a structural understanding of interactions with G proteins is lacking. This is largely due to the highly flexible nature of the CB1 Ct that dynamically adapts its conformation to the presence of G proteins. In the present study, we explored how the CB1 Ct can interact with the G protein by building on our prior modeling of the CB1-Gi complex (Shim J-Y, Ahn KH, Kendall DA. The Journal of Biological Chemistry 2013;288:32449-32465) to incorporate a complete CB1 Ct ($Glu416^{Ct}$–$Leu472^{Ct}$). Based upon the structural constraints from NMR studies, we employed ROSETTA to predict tertiary folds, ZDOCK to predict docking orientation, and molecular dynamics (MD) simulations to obtain two distinct plausible models of CB1 Ct in the CB1-Gi complex. The resulting models were consistent with the NMR-determined helical structure (H9) in the middle region of the CB1 Ct. The CB1 Ct directly interacted with both Gα and Gβ and stabilized the receptor at the Gi interface. The results of site-directed mutagenesis studies of $Glu416^{Ct}$, $Asp423^{Ct}$, $Asp428^{Ct}$, and $Arg444^{Ct}$ of CB1 Ct suggested that the CB1 Ct can influence receptor-G protein coupling by stabilizing the receptor at the Gi interface. This research provided, for the first time, models of the CB1 Ct in contact with the G protein.

### Keywords

cannabinoid receptor; carboxyl-terminus; G protein coupling; protein structure; molecular dynamics; site-directed mutagenesis; G protein-coupled receptor (GPCR)

## Introduction

Agonist-stimulated G protein-coupled receptors (GPCRs) interact with G proteins and trigger a series of internal G protein-dependent signaling events (for a review, see ref. 1). These agonist-stimulated GPCRs are also phosphorylated by GPCR kinases (GRKs)[2] which facilitate G protein uncoupling and arrestin recruitment, leading to receptor desensitization and internalization[3-6]. The X-ray crystal structure of the agonist-bound β2-adrenergic

[*]Author to whom correspondence should be addressed: joong@email.unc.edu.

Conflicts of interest

The authors declare that they have no conflicts of interest with the contents of this article.

receptor (β2AR) in complex with Gs[7] revealed the molecular details of the GPCR-G protein interaction where the C-terminal helix α5 of Gα binds to the intracellular (IC) core of the receptor. A recent X-ray crystal structure of the finger loop peptide of rod photoreceptor arrestin (S-arrestin) bound to rhodopsin[8] showed that arrestins also utilize the same receptor IC core as a key contact. This suggests that G proteins and arrestins compete for a common binding site on the activated receptor. Although little is known about the molecular details of how a GPCR interacts with GRKs, partly due to relatively low affinity for the formation of the GPCR-GRK complex[9], it has been proposed that the N-terminal helix of the kinase domain of GRKs also interact with the same IC core of the activated receptor[10].

Deletion or mutation of the cytoplasmic carboxyl-terminus (Ct) in GPCRs impaired not only G protein coupling but also internalization and desensitization[11-16], suggesting that the receptor Ct plays a crucial role in the regulation of G protein signaling. Ct in GPCRs is also an important site for the interactions with GRKs and arrestins[2,4,5]. A very recent X-ray crystal structure of a constitutively active form of rhodopsin bound to mouse visual arrestin[17] revealed that the Ct forms an interface patch for the interaction of rhodopsin with arrestin, which was validated by extensive cross-linking between the N-terminus of arrestin and Ct of rhodopsin. It was suggested that the phosphorylated Ct of the receptor can form tight interactions with the positively charged pockets of the N-terminus of arrestin, thus emphasizing the critical role of Ct. Similar charge-charge interactions between the phosphorylated Ct peptide and positively charged resides of β-arrestin-1 were also suggested in the X-ray crystal structure of the phosphorylated Ct peptide of the human V2 vasopressin receptor (V2R) bound to β-arrestin-1[18]. It is remarkable that different regions of the receptor Ct play distinct roles in signal regulation. For example, it was shown in the human neuropeptide Y receptor type 2 (Y2R) that the N-terminal region of the Ct was involved in internalization in a β-arrestin-independent manner, the C-terminal region of the Ct was involved in internalization in a β-arrestin-dependent manner, and the middle region of Ct was involved in regulating the activity of the first two regions[13]. It was also shown in the β2AR that the N-terminal region of the Ct contained the GRK6 phosphorylation sites responsible for β-arrestin-mediated ERK activation, while the C-terminal region of Ct contained the GRK2 phosphorylation site responsible for internalization[19]. Similarly, mutagenesis studies of the μ opioid receptor (MOR) Ct indicated that different kinases phosphorylated different Ser residues[20]. These results suggest that recruitment of specific types of GRKs and β-arrestins is dictated by the conformation of the GPCR carboxyl-terminus. Thus, the finding that carvedilol, a β-arrestin-biased ligand, induced phosphorylation of β2AR only by GRK6, while isoproterenol, a non-biased ligand, induced phosphorylation of β2AR both by GRK2 and GRK6[19] suggests that the ligand likely puts the receptor in a distinct conformation that induces a specific profile of phosphorylation of the Ct.

The brain cannabinoid receptor one (CB1) is a rhodopsin subfamily (class A) GPCR found predominantly in the central nervous system (CNS)[21]. As in many GPCRs, CB1 Ct has been shown to be important for G protein signal regulation (for review, see ref. 22). A series of truncation mutants were studied to examine the functional importance of CB1 Ct. Deletion of the entire Ct including the juxta-membrane eighth helix (H8) that follows the transmembrane (TM) helical domain resulted in abolished $Ca^{2+}$ channel inhibition[23].

Moreover, the removal of Arg400$^{H8}$ from a peptide analog of H8 of the CB1 receptor exhibited a 6-fold reduction in Gi affinity and an almost complete loss of the inhibitory effect on adenylyl cyclase activity[24]. These results suggest that H8 plays an important role in G protein coupling to the CB1 receptor. Our recent computational modeling study of the CB1-Gi complex identified Arg400$^{H8}$ as one of the key CB1 contact residues with the C-terminal helix α5 of Gα at the receptor-Gi interface[25]. Interestingly, truncation of the Ct at position Thr418$^{Ct}$ immediately after H8 exhibited an increase in constitutive activity and G protein sequestration[26], suggesting that CB1 Ct after H8 plays a role in regulating G protein activation. Different sections of CB1 Ct play distinct roles in signal regulation. It was observed that Ala mutations of Ser425$^{Ct}$ and/or Ser429$^{Ct}$ at the N-terminal region of CB1 Ct resulted in significant decreases (> 50%) in GRK3- and β-arrestin 2-mediated desensitization[27] and delayed tolerance[28]. Furthermore, biochemical studies of the truncation and multiple Ala mutations indicated that Ser and Thr residues (Thr460$^{Ct}$–Ser468$^{Ct}$) at the C-terminal region of CB1 Ct were important for receptor internalization[29].

While increasing information is available for the structure of extracellular (EC) and TM domains of GPCRs, only limited information is available for the structure of GPCR Ct. No X-ray crystal structure of any GPCR, where the receptor Ct is complete, has ever been determined, since the receptor structure beyond H8 is frequently disordered due to its intrinsic flexibility[30]. The X-ray crystal structures of rhodopsin (pdb codes 1U19 and 3AYN)[31,32] revealed that the Ct was folded under the receptor IC surface, particularly near H8. In contrast, the conformation of β2AR Ct was suggested to be extended and unstructured from fluorescence resonance energy transfer (FRET) studies[33], which would be important for inducing distinct conformations by different ligands[19].

Without having any X-ray crystal structure of CB1 Ct, Ahn et al.[34] determined the NMR structure of the unphosphorylated CB1 Ct peptide (Arg400$^{H8}$–Leu472$^{Ct}$). They identified a helix (Ala440$^{Ct}$–Met461$^{Ct}$) called the ninth helix (H9) in the middle region (Table 1). Two additional NMR structures of phosphorylated CB1 Ct peptides in complex with human β-arrestin-1 have been reported. The NMR structure of the diphosphorylated CB1 Ct peptide (residues Thr418$^{Ct}$–Asn437$^{Ct}$) in complex with β-arrestin-1[35] showed two helical segments (Leu422$^{Ct}$–Gly427$^{Ct}$ and Asp428$^{Ct}$–Leu432$^{Ct}$) (Table 1). A more recent NMR study on the pentaphosphorylated, extreme C-terminal peptide (residues Thr453$^{Ct}$–Leu472$^{Ct}$) in complex with β-arrestin-1[36] revealed the presence of a helical segment (Asp466$^{Ct}$–Glu470$^{Ct}$) (Table 1). These NMR-determined secondary structures of CB1 Ct are intriguing in that well-defined secondary structures and/or folds can be induced from the intrinsically disordered CB1 Ct upon interaction with its cognate binding proteins (the G protein, GRKs and arrestin) and in that the nature of phosphorylation would significantly alter the secondary structure and fold, and thereby the function, of CB1 Ct.

Although these NMR studies[34-36] provided invaluable insight into the CB1 Ct peptide structure, it is necessary to determine the structure of CB1 Ct in contact with the G protein to gain structural information about the potential role of CB1 Ct in G protein signaling. In this study, we elucidated the plausible interactions of CB1 Ct with the G protein by building on our prior modeling effort of the CB1-Gi complex lacking CB1 Ct (CB1(**no$^{Ct}$**)-Gi)[25]. The

results suggested that the CB1 Ct can influence receptor-G protein coupling by stabilizing the receptor at the Gi interface.

## Methods

### Cell Culture and Membrane Preparation

HEK293 cells were transiently transfected with the wild-type or mutant CB1 receptor using the calcium phosphate precipitation method as described previously[37]. One day after transfection, membrane preparations were made[38]. This involved washing the cells with phosphate buffered saline (PBS) and resuspending them in a solution of PBS with 1% (v/v) protease inhibitor cocktail (Sigma-Aldrich, St. Louis, MO). The cells were subjected to nitrogen cavitation at 750 psi using a Par cell disruption bomb. The disrupted cells were then centrifuged at 500 × *g* for 10 min at 4°C and the supernatant was extracted. The supernatant was then centrifuged at 100,000 × *g* for 45 min at 4°C and the membrane pelleted. The membrane pellet was resuspended in TME buffer (25 mM Tris-HCl, 5 mM $MgCl_2$, and 1 mM EDTA, pH 7.4) with 7% (w/v) sucrose and the protein concentration was determined using the Bradford assay[39].

### Ligand Binding Assay

Competition binding assays were performed as described previously[40]. Briefly, 7.5 μg of wild-type or mutant CB1 receptor membrane preparations were incubated for 60 min with increasing concentrations of CP55,940 ranging between 100 *p*M and 10 μM in the presence of 2 nM [$^3$H]CP55,940 (141 Ci/mmol, PerkinElmer Life Sciences (Boston, MA)) as tracer in a total volume of 200 μl of TME buffer containing 0.1% fatty acid-free BSA. Nonspecific binding was assessed using 1 μM unlabeled CP55,940. The reaction was terminated by the addition of 250 μl TME buffer containing 5% BSA followed by filtration with a Brandel cell harvester through Whatman GF/C filter paper and the bound radioactivity measured. Ligand depletion was avoided and the bound ligand was kept less than 10% of the total.

### GTPγS Assay

Briefly, 8.5 μg of membrane preparation was tested with at least nine different concentrations of unlabeled CP55,940 ranging between 100 *p*M and 10 μM as described previously[40]. The membrane preparations were incubated with 0.1 nM [$^{35}$S] GTPγS (1,250 Ci/mmol; PerkinElmer Life Sciences, Boston, MA), 3 μM GDP (Sigma, St. Louis, MA), 0.1% w/v BSA and varying concentrations of unlabeled CP55,940 in a total volume of 200 μl of GTPγS binding buffer (50 mM Tris-HCl, pH 7.4, 3 mM $MgCl_2$, 0.2 mM EGTA and 100 mM NaCl) for 60 min. Nonspecific binding was determined with 10 μM unlabeled GTPγS (Sigma, St. Louis, MA). The reaction was terminated by filtration through Whatman GF/C filters followed by washing with ice cold TME buffer and the bound radioactivity determined.

### Data Analysis

All ligand binding and GTPγS assays were carried out in duplicate and at least three independent experiments were performed. Data are presented as the mean ± S.E. for the $K_i$ values, basal levels and CP55,940-induced $E_{max}$ values and the median and the

corresponding 95% confidence limits for the $EC_{50}$ values. The data collected were subjected to nonlinear regression using Prism 6.0 (Graphpad Software Inc., San Diego, CA) as previously described[41]. Comparison was done using analysis of variance (ANOVA) between the wild type and the mutant receptors followed by Bonferroni's post hoc test and $p < 0.05$ was considered statistically significant.

## Generation of Tertiary Folds of the CB1 Carboxyl-terminus

Using ROSETTA's comparative modeling protocols[42,43], we sampled the conformational space related to the sequence of the CB1 Ct peptide ($Glu416^{Ct}$–$Leu472^{Ct}$) and obtained the structural backbone of the CB1 Ct peptide from a fragment library extracted from known protein structures using Monte Carlo sampling[44]. We also sampled side chain conformation of the CB1 Ct peptide using the rotamer database[45] and obtained the best combination of side chain angles by Monte Carlo simulated annealing. Among the highest scored ROSETTA-predicted models, we selected five models that agreed with NMR data[34-36].

## Docking of CB1 Ct to the CB1-Gi Complex

Each of the five ROSETTA-predicted models of the CB1 Ct peptide was docked to our prior model of the CB1-Gi complex (CB1($\mathbf{no^{Ct}}$)-Gi)[25], where the CB1 receptor was truncated at the palmitoylated $Cys415^{H8}$ at the end of H8, using the ZDOCK (version 3.0.2) server[46]. We examined the ZDOCK models of the CB1 Ct peptide in the CB1-Gi complex and selected the best model using the following criteria: i) the fifty best scoring ZDOCK models of the CB1 Ct peptide in the CB1-Gi complex were selected; ii) the distance between the C-terminal end residue ($Cys415^{H8}$) of the CB1 receptor and the N-terminal end residue ($Glu416^{Ct}$) of the docked CB1 Ct peptide should be less than 10 Å, a loose distance criteria between these residues for the formation of the amide bond in the following step for completing the receptor Ct (see below); and iii) the docked CB1 Ct peptide should not be in unfavorable contacts with any part of both the receptor and the G protein. We repeated this docking procedure for all of the five ROSETTA-predicted models of the CB1 Ct peptide. The best two ROSETTA-predicted models of the CB1 Ct peptide in the CB1-Gi complex that met the above criteria were selected. We called these two plausible models of CB1 Ct in the CB1-Gi complex, $\mathbf{A^{Ct}}$ and $\mathbf{B^{Ct}}$.

## Simulations of the CB1-Gi Complex

### Simulations of the CB1 Ct peptide and the CB1-Gi complex (CB1($\mathbf{no^{Ct}}$)-Gi)—

Each of the CB1 Ct peptides, $\mathbf{A^{Ct}}$ and $\mathbf{B^{Ct}}$, were inserted into our prior model of the CB1-Gi complex (CB1($\mathbf{no^{Ct}}$)-Gi) in a fully hydrated 1-palmitoyl-2-oleoyl-*sn*-glycero-3-phosphocholine (POPC) lipid bilayer[25]. The N-terminus of the CB1 Ct peptide was capped by an acetyl group, while the C-terminus was retained as a free carboxylate form. Any water molecule within 1.0 Å of the newly added CB1 Ct peptide was removed. The system was then electrically neutralized (to ~0.15 M NaCl) using the Solvate plugin in VMD[47]. A total of ~220,000 atoms, including the cannabinoid agonist (−)-11-hydroxydimethylheptyl-$\Delta^8$-tetrahydrocannabinol (HU210)-bound whole CB1 receptor, the GDP-bound Gi protein, 73 $Na^+$ and 69 $Cl^-$ ions, ~51,300 water molecules, and ~360 POPC molecules, resulted in a system of the CB1-Gi complex (Fig. 1A i and 1B i) in a simulation box of approximately 90

× 130 × 180 Å$^3$. The entire system of the CB1-Gi complex was subjected to energy minimization (3,000 iterations). This was followed by two distance-restrained MD simulations at 310 K in the NPT ensemble: The distance between the backbone carbonyl oxygen atom of Cys415$^{H8}$ in the CB1 receptor and the backbone amide nitrogen atom of Glu416$^{Ct}$ in the CB1 Ct peptide was harmonically constrained (20.0 kcal/molÅ$^2$) to 10 Å for the first 5 ns of the simulation and to 5 Å for the second 5 ns of the simulation.

**Simulations of the CB1-Gi complexes CB1(A$^{Ct}$)-Gi and CB1(B$^{Ct}$)-Gi—**For the resulting system, we created an amide bond between the receptor C-terminal Cys415$^{H8}$ in the CB1-Gi complex model and the N-terminal Glu416$^{Ct}$ of the CB1 Ct peptide to complete the receptor within the CB1-Gi complex. Then, the entire system of the CB1-Gi complex was subjected to an energy minimization (3,000 iterations). This was followed by a simulation at 310 K in the NPT ensemble to obtain an all-atom, solvent-equilibrated model of the CB1-Gi complex. By repeating this step for each of **A$^{Ct}$** and **B$^{Ct}$**, we obtained two distinct models of CB1 Ct in the CB1-Gi complex, CB1(**A$^{Ct}$**)-Gi and CB1(**B$^{Ct}$**)-Gi.

### Simulation Protocol

All simulations were performed using the NAMD simulation package (ver. 2.7 Linux-x86_64)[48], using CHARMM36 force field parameters for proteins with the ϕ/ψ angle cross-term map correction[49,50] and lipids[51], and the TIP3P water model[52]. The temperature was maintained at 310 K through the use of Langevin dynamics[53] with a damping coefficient of 1/ps. The pressure was maintained at 1 atm by using the Nosé-Hoover method[54] with the modifications as described in the NAMD user's guide. The van der Waals interactions were switched at 10 Å and zero smoothly at 12 Å. Electrostatic interactions were treated using the Particle Mesh Ewald (PME) method[55]. A pair list for calculating the van der Waals and electrostatic interactions was set to 13.5 Å and updated every 10 steps. A multiple time-stepping integration scheme, the impulse-based Verlet-I reversible reference system propagation algorithm method[56], was used to efficiently compute full electrostatics. The time step size for integration of each step of the simulation was 1 fs.

## Results

### Structural Stability of CB1 Ct in the CB1-Gi Complex

Two all-atom, solvent-equilibrated models of the CB1-Gi complex, CB1(**A$^{Ct}$**)-Gi and CB1(**B$^{Ct}$**)-Gi, at the end of 205 ns simulations are shown in Fig. 1A i and 1B i respectively. At the end of the simulations, no residue of **A$^{Ct}$** or **B$^{Ct}$** was in the disallowed region on the Ramanchandran plot as defined by PROCHECK[57]. To measure the structural stability of CB1(**A$^{Ct}$**)-Gi and CB1(**B$^{Ct}$**)-Gi, the root-mean-square deviations (RMSDs) were calculated over the performed simulations (Fig. 1A ii and 1B ii). The RMSD values of both models of the whole complex continued to evolve without being fully stabilized by the end of the simulation. However, the RMSD values of **A$^{Ct}$** in CB1(**A$^{Ct}$**)-Gi indicated that the CB1 Ct was fully stabilized after 175 ns of the simulation (Fig. 1A ii). At ~175 ns of the simulation, the RMSD values of **A$^{Ct}$** were slightly increased when part of the structural motifs of **A$^{Ct}$** was rearranged in response to the extreme C-terminal end residue Leu472$^{Ct}$ that became deeply inserted into the CB1-Gα/Gβ interfacial region and formed tight salt bridges to

R336$^{IC3}$ and R340$^{IC3}$ of the CB1 receptor (Fig. 1A iii). In contrast to **A$^{Ct}$** in CB1(**A$^{Ct}$**)-Gi, **B$^{Ct}$** in CB1(**B$^{Ct}$**)-Gi was not completely stabilized at the end of 205 ns simulations (Fig. 1B ii). In **B$^{Ct}$**, the highly flexible C-terminal end residue Leu472$^{Ct}$ that traveled over 40 Å and formed tight salt bridges to R405$^{H8}$ of the CB1 receptor near the TM7/H8 junction (Fig. 1B iii).

## Molecular Features of the CB1 Ct

**A$^{Ct}$** in CB1(**A$^{Ct}$**)-Gi contained one helical segment (H9) in the middle region adjacent to three anti-parallel β-bridges in both the N- and C-terminal regions (Fig. 1A i), while **B$^{Ct}$** in CB1(**B$^{Ct}$**)-Gi contained H9 in the middle region and another helical segment in the N-terminal region (Fig. 1B i). In both models, H9, largely in agreement with the NMR-structure of the CB1 Ct peptide[34] (Table 1), was in an amphipathic alignment: the nonpolar face was buried and participated in forming the extensive hydrophobic cluster (Fig. 2A), while the polar face was exposed to the solvent. The detailed interactions of the CB1 Ct within the CB1-Gi complex are listed in Table 2. Throughout the simulations of CB1(**A$^{Ct}$**)-Gi and CB1(**B$^{Ct}$**)-Gi, H9 in the middle region of CB1 Ct were well retained. One of the reasons that the helical contents of H9 in the present models were more limited (<15 residue-long) compared with the NMR-determined structure (22 residue-long)[34] was that H9 in the present models of CB1 Ct was stabilized in an intact receptor environment, while the NMR-determined structure was stabilized in a dodecylphospho-choline (DPC) micelle environment[34], a media favorable for helical induction. **B$^{Ct}$** agreed with the NMR structure of the CB1 Ct peptide[35] with respect to the presence of an additional helix on the N-terminal region of CB1 Ct (Table 1). In CB1(**B$^{Ct}$**)-Gi, this additional helix was created during the simulation (Fig. 2B), suggesting the N-terminal region of CB1 Ct has a tendency to have a helical structure. None of the present models of CB1 Ct predicted the presence of the helical segment at the C-terminal region identified in one NMR structure[36] (Table 1). This may be due to the fact that the NMR structure was multi-phosphorylated and in complex with arrestins, while the present structure was unphosphorylated and in complex with the G protein.

## Flexibility of CB1 Ct in the CB1-Gi Complex

To examine the intrinsic flexibility of CB1 Ct in the CB1-Gi complex, we calculated the variance of every atom position over the trajectories of the last 20 ns of the simulation for each of CB1(**A$^{Ct}$**)-Gi and CB1(**B$^{Ct}$**)-Gi. The RMS fluctuation (RMSF) plots (Fig. 3) indicated that CB1 Ct was one of the most flexible regions in the CB1-Gi complex. The only region equally flexible to CB1 Ct was the 40 residue-long third IC loop (IC3) of the CB1 receptor and the α-helical domain of Gα that is crucial for G protein activation[1]. Comparison of the RMSF plots of CB1(**A$^{Ct}$**)-Gi and CB1(**B$^{Ct}$**)-Gi revealed that the middle region of **A$^{Ct}$** highly fluctuated compared with that of **B$^{Ct}$** (Fig. 3). Since the N-terminal region is directly connected to the middle region, fluctuations in the N-terminal region would contribute to fluctuations in the middle region. Thus, the less structured N-terminal region of **A$^{Ct}$** in CB1(**A$^{Ct}$**)-Gi compared with the more structured N-terminal region of **B$^{Ct}$** in CB1(**B$^{Ct}$**)-Gi (Table 1) would give rise to high fluctuations in the middle region of **A$^{Ct}$** in CB1(**A$^{Ct}$**)-Gi.

### Site-directed Mutagenesis Studies of Glu416$^{Ct}$, Asp423$^{Ct}$, Asp428$^{Ct}$, and Arg444$^{Ct}$ of CB1 Ct in the CB1-Gi Complex

To investigate the potential role of CB1 Ct in the G protein coupling activity, we chose four amino acid residues, Glu416$^{Ct}$, Asp423$^{Ct}$, Asp428$^{Ct}$, and Arg444$^{Ct}$, from the CB1 Ct which were suggested to be important for intra- or inter-molecular interactions in stabilizing the CB1-Gi complex (Table 2). Both Glu416$^{Ct}$ and Asp428$^{Ct}$ were suggested to form charged-charged intra-molecular interactions with Arg409$^{H8}$ in both CB1(**A$^{Ct}$**)-Gi and CB1(**B$^{Ct}$**)-Gi (Table 2), stabilizing H8 of the receptor. Asp428$^{Ct}$ was also involved in stabilizing the structured motifs in the middle region of the CB1 Ct in CB1(**A$^{Ct}$**)-Gi. We chose Asp423$^{Ct}$, which was suggested to have inter-molecular interactions with Gβ in both CB1(**A$^{Ct}$**)-Gi and CB1(**B$^{Ct}$**)-Gi (Table 2). Arg444$^{Ct}$ was suggested to have intra-molecular interactions with Glu447$^{Ct}$, stabilizing the middle region α-helix in CB1(**A$^{Ct}$**)-Gi and with Asp466$^{Ct}$, stabilizing the C-terminal end region in CB1(**B$^{Ct}$**)-Gi (Table 2). These residues were frequently involved in tight salt bridges in the present models of the CB1-Gi complex (Table 2), suggesting that the disruption of these residues may cause destabilization of CB1 Ct.

In ligand binding experiments, the four mutated receptors showed no difference in the $K_i$ values for binding of CP55,940 compared to wild-type CB1 (Table 3 and Fig. 4A), suggesting no impact of these mutations on the folding, conformational stability and expression of these receptors. These mutated receptors were then analyzed for their G protein coupling activity. First, we evaluated the $EC_{50}$ values for CP55,940-induced G protein coupling. None of the mutated receptors showed any significant difference in the concentration of CP55,940 ($EC_{50}$ values) needed for G protein coupling compared to the wild-type CB1 receptor (Table 3 and Fig. 4B). Second, we analyzed the level of G protein coupling for basal activity (CB1 exhibits some constitutive activity in the absence of ligand[58,59]). There was no significant impact on the basal level of GTPγS binding for the Glu416$^{Ct}$Ala receptor suggesting that G protein coupling was essentially the same as the wild-type CB1 receptor. Interestingly, the basal levels of Asp423$^{Ct}$Ala and Asp428$^{Ct}$Ala receptors were significantly higher compared to the wild-type CB1 receptor. In contrast, the basal level of Arg444$^{Ct}$Ala receptor was not significantly different from the wild-type CB1 receptor (Table 3 and Fig. 4B). Third, we evaluated the impact of these mutations on the $E_{max}$ levels for G protein coupling following CP55,940 treatment. Treatment with agonists like CP55,940 allows the receptor to adopt an active confirmation, thus revealing maximal G protein coupling by that ligand as depicted by the $E_{max}$ levels. No change in the $E_{max}$ levels was observed for Glu416$^{Ct}$Ala compared to the wild-type CB1 receptor, suggesting that this residue may be less important for G protein coupling. Interestingly, the $E_{max}$ level for the Arg444$^{Ct}$Ala receptor was somewhat lower than the wild-type CB1 receptor suggesting that G protein coupling is impaired by this mutation. On the other hand, the $E_{max}$ levels for the Asp423$^{Ct}$Ala and Asp428$^{Ct}$Ala receptors following CP55,940 treatment, were higher than the wild-type CB1 receptor. Thus, this suggests that the residue replacements by these mutations promote G protein coupling, which is reflected in both basal and CP55,940-induced levels. Overall, none of the mutations impacted the concentration of CP55,940 needed to get half maximal G protein coupling though some did impact the maximum extent of G protein coupling suggesting the efficacy of G protein coupling was altered.

## Discussion

CB1 Ct has been shown to be important for G protein signal regulation (for review, see ref. 22). Since the CB1 Ct is highly flexible, its position and conformation easily adapt to the presence of G proteins. In order to understand the role of CB1 Ct in G protein coupling, we explored the structure of the 57-residue ($Glu416^{Ct}$–$Leu472^{Ct}$) CB1 Ct in the CB1-Gi complex. Full conformational sampling of CB1 Ct is almost impossible due to the large number of degrees of freedom. Earlier work showed that the 25 residue-long rhodopsin Ct was not well sampled by 26 independently constructed simulations of rhodopsin embedded in an explicit lipid membrane on the 100 ns time scale[59]. Enhanced sampling techniques, such as replica exchange molecular dynamics (REMD)[60,61], have been widely used for enhancing the conformational sampling of MD simulations. However, even an explicit solvent system for a small protein (~ 20 residue-long) requires more than 40 replicas for efficient REMD[62]. Moreover, the simulations time should be long enough for each trajectory to cover the entire conformational space as well as the entire temperature space[63].

Exhaustive sampling was not used in the present study because we aimed to obtain a plausible and reasonable model view for the structure of the contact region of the CB1 Ct with the G protein. To mitigate the problem in conformational sampling, we employed ROSETTA to predict tertiary folds of the CB1 Ct peptide, ZDOCK to predict docking orientations of CB1 Ct considering the structural constraints imposed as part of the CB1 receptor in the CB1-Gi complex. ROSETTA has been reputed to predict high-probability structures of protein domains with fewer than 200 amino acid de novo[64], while ZDOCK has demonstrated its high performance in predicting protein–protein docking orientation with > 60% success in Critical Assessment of Predicted Interactions (CAPRI)[65]. Owing to the motion of the intrinsically flexible CB1 Ct, the trajectories produced by independent simulations of two distinct models of CB1 Ct in two different regions of the configuration space of the CB1-Gi complex appeared to enable sampling of regions that otherwise would be little visited. For example, in CB1($\mathbf{B}^{\mathbf{Ct}}$)-Gi, the performed simulations enabled freely visiting most of the region of Ct fold (*i.e.* the CB1-Gα/Gβ interface under the receptor IC surface) (Fig. 2B).

RMSDs calculated only for secondary structure were used to measure the structural stability of CB1($\mathbf{A}^{\mathbf{Ct}}$)-Gi and CB1($\mathbf{B}^{\mathbf{Ct}}$)-Gi. It appeared that the structural motifs in the middle region played a pivotal role in determining the overall stability of CB1 Ct in the CB1-Gi complex. However, the stability of the structural motifs in the middle region appeared to be influenced by the highly flexible C-terminal region that is tethered to these structural motifs. Indeed, the structural motifs in the middle region were frequently rearranged adapting to the formation of tight salt bridges by the extreme C-terminal end residue $Leu472^{Ct}$ at the CB1-Gα/Gβ interfacial region (Fig. 1A i and 1B i). Possibly due to the highly flexible nature of the Gα-Gβ interfacial region as well as the unstructured regions of CB1 Ct (both the N-terminal and C-terminal regions), substantially long simulations of the present models of the CB1-Gi complex are needed in future studies for a full structural convergence of CB1 Ct.

Intrigued by a strong tendency of the extreme C-terminal end residue $Leu472^{Ct}$ to form salt bridges to the CB1-Gα/Gβ interfacial region (Fig. 1A iii and 1B iii), we examined the

electrostatic surface map of the CB1-Gi complex (Fig. 2C i). It revealed that the CB1-Gα/Gβ interfacial region was electrostatically highly positive. Since the extreme C-terminal residue Leu472$^{Ct}$ was free to move, the negatively charged carboxylate moiety of Leu472$^{Ct}$ was facilitated to come in close proximity to this highly electrostatically-positive receptor-Gα/Gβ interfacial region (Fig. 2C i). The electrostatic surface map of the CB1-Gi complex also revealed that the Gβ region that formed one of the main contacts with the structural motifs in the middle of CB1 Ct was electrostatically highly negative (Fig. 2C i). It was indicated that the electrostatic surface map of the structural motifs in the middle region of **B$^{Ct}$** was poorly matched to the electrostatically negative Gβ region (Fig. 2C ii), suggesting that **B$^{Ct}$** in CB1(**B$^{Ct}$**)-Gi was not close to a structural convergence (Fig. 1B ii).

A combined analysis of the computational models of the CB1 Ct and the results of site-directed mutagenesis studies of Glu416$^{Ct}$Ala, Asp423$^{Ct}$Ala, Asp428$^{Ct}$Ala and Arg444$^{Ct}$Ala mutant receptors suggested that the CB1 Ct can influence receptor-G protein coupling by stabilizing the receptor at the CB1-Gi interface. 1) **Interaction with the receptor at the Gα interface**. The CB1 Ct can influence receptor-G protein coupling by stabilizing the receptor at the Gα interface, as suggested by the mutagenesis results of Arg428$^{Ct}$Ala mutant receptor. Similarly, the carboxylate of Leu472$^{Ct}$ of the CB1 Ct appeared to stabilize the receptor at the Gα interface (Fig. 1B i and ii). 2) **Interaction with Gα.** It was shown that the CB1 Ct commonly formed a couple of charge-charge interactions with Gα (Table 2), which could affect G protein coupling. 3) **Interaction with Gβ**. The CB1 Ct can exert its role in receptor-G protein coupling indirectly through the interactions with Gβ, as suggested by the mutagenesis results of Asp423$^{Ct}$Ala mutant receptor. 4) **Intra-molecular interaction within CB1**. The intra-molecular interactions within CB1 that stabilize the CB1 Ct are also indirectly important for maintaining the conformation of CB1 that forms a complex with G protein, as suggested by the Arg444$^{Ct}$Ala mutant receptor. Overall, it appeared that the CB1 Ct can influence receptor-G protein coupling through a combination of different ways of stabilizing the receptor at the CB1-Gi interface.

In summary, we explored how the CB1 Ct can interact with G protein. A combined analysis of the two distinct models of CB1 Ct suggested that the CB1 Ct can influence receptor-G protein coupling by stabilizing the receptor at the CB1-Gi interface. This research provided, for the first time, models of CB1 Ct in contact with the G protein.

## Acknowledgements

This work was partially supported by the National Institutes of Health Grant DA020663 (to J.-Y. S.) and Grant DA020763 (to D.A.K). This work used the Extreme Science and Engineering Discovery Environment (XSEDE) (to J.-Y.S.), which is supported by National Science Foundation under Grant No. OCI-1053575. The Texas Advanced Computing Center (TACC) at The University of Texas at Austin is greatly acknowledged for providing HPC resources that have contributed to the research results reported within this paper. This work used Big Red at Indiana University, which was supported by the National Science Foundation under Grant No. ACI-0338618l, OCI-0451237, OCI-0535258, and OCI-0504075.

## Abbreviations

The abbreviations used are:

| | |
|---|---|
| **CB1 receptor** | cannabinoid receptor one |

| | |
|---|---|
| **GPCR** | G protein coupled receptor |
| **HU210** | (−)-11-hydroxydimethylheptyl-$\Delta^8$-tetrahydrocannabinol |
| **TM** | transmembrane |
| **IC** | intracellular |
| **β2AR** | β2 adrenergic receptor |
| **FRET** | fluorescence resonance energy transfer |
| **MD** | molecular dynamics |
| **HEK293** | human embryonic kidney cell |
| **PBS** | phosphate-buffered saline |
| **TME** | Tris/$Mg^{2+}$/EDTA |
| **GRK** | G protein-coupled receptor kinases |
| **ERK** | extracellular signal-regulated kinases |
| **GTPγS** | guanosine 5′-3-O-(thio)triphosphate |
| **CP55,940** | (1R, 3R, 4R)-3-[2-hydroxy-4-(1,1-dimethylheptyl)phenyl]-4-(3-hydrxypropyl)cyclohexan-1-ol |
| **GDP** | guanosine diphosphate |
| **Y2R** | neuropeptide Y receptor type 2 |
| **V2R** | V2 vasopressin receptor |
| **MOR** | the μ opioid receptor |
| **POPC** | 1-palmitoyl-2-oleoyl-*sn*-glycero-3-phosphocholine |
| **DPC** | dodecylphosphocholine |
| **PME** | Particle Mesh Ewald |
| **PAL** | palmitoyl moiety |
| **GER** | geranylgeranyl moiety |
| **RMSDs** | the root-mean-square deviations |
| **RMSF** | root-mean-square fluctuation |
| **Ct** | carboxyl-terminus |
| **CNS** | central nervous system |
| **CAPRI** | critical assessment of predicted interactions |

| | |
|---|---|
| **VMD** | visual molecular dynamics |
| **APBS** | adaptive Poisson-Boltzmann solver |
| **REMD** | replica exchange molecular dynamics |

## References


1. Oldham WM, Hamm HE. Heterotrimeric G protein activation by G-protein-coupled receptors. Nature Reviews Molecular Cell Biology. 2008; 9:60–71. [PubMed: 18043707]
2. Pao CS, Benovic JL. Phosphorylation-independent desensitization of G protein-coupled receptors? Science STKE. 2002:pe42.
3. Shenoy SK, Lefkowitz RJ. Seven-transmembrane receptor signaling through beta-arrestin. Science STKE. 2005:cm10.
4. Premont RT, Gainetdinov RR. Physiological roles of G protein-coupled receptor kinases and arrestins. Annual Review of Physiology. 2007; 69:511–534.
5. Reiter E, Ahn S, Shukla AK, Lefkowitz RJ. Molecular mechanism of β-arrestin-biased agonism at seven-transmembrane receptors. Annual Review of Pharmacology and Toxicology. 2012; 52:179–197.
6. Gurevich EV, Tesmer JJ, Mushegian A, Gurevich VV. G protein-coupled receptor kinases: more than just kinases and not only for GPCRs. Pharmacology & Therapeutics. 2012; 133:40–69. [PubMed: 21903131]
7. Rasmussen SG, DeVree BT, Zou Y, Kruse AC, Chung KY, Kobilka TS, Thian FS, Chae PS, Pardon E, Calinski D, Mathiesen JM, Shah ST, Lyons JA, Caffrey M, Gellman SH, Steyaert J, Skiniotis G, Weis WI, Sunahara RK, Kobilka BK. Crystal structure of the β2 adrenergic receptor-Gs protein complex. Nature. 2011; 477:549–555. [PubMed: 21772288]
8. Szczepek M, Beyrière F, Hofmann KP, Elgeti M, Kazmin R, Rose A, Bartl FJ, von Stetten D, Heck M, Sommer ME, Hildebrand PW, Scheerer P. Crystal structure of a common GPCR-binding interface for G protein and arrestin. Nature Communications. 2014; 5:4801.
9. Tesmer, JJG. Activation of G protein-coupled receptor (GPCR) kinases by GPCRs. In: Giraldo, J., Pin, J-P., editors. G Protein-Coupled Receptors: From Structure to Function. RSC Publishing; 2011. p. 297-315.
10. Huang CC, Tesmer JJ. Recognition in the face of diversity: interactions of heterotrimeric G proteins and G protein-coupled receptor (GPCR) kinases with activated GPCRs. The Journal of Biological Chemistry. 2011; 286:7715–7721. [PubMed: 21199869]
11. Reneke JE, Blumer KJ, Courchesne WE, Thorner J. The carboxy-terminal segment of the yeast alpha-factor receptor is a regulatory domain. Cell. 1988; 55:221–234. [PubMed: 2844413]
12. Matus-Leibovitch N, Nussenzveig DR, Gershengorn MC, Oron Y. Truncation of the thyrotropin-releasing hormone receptor carboxyl tail causes constitutive activity and leads to impaired responsiveness in Xenopus oocytes and AtT20 cells. The Journal of Biological Chemistry. 1995; 270:1041–1047. [PubMed: 7836357]
13. Walther C, Nagel S, Gimenez LE, Mörl K, Gurevich VV, Beck-Sickinger AG. Ligand-induced internalization and recycling of the human neuropeptide Y2 receptor is regulated by its carboxyl-terminal tail. The Journal of Biological Chemistry. 2010; 285:41578–41590. [PubMed: 20959467]
14. Bouvier M, Hausdorff WP, De Blasi A, O'Dowd BF, Kobilka BK, Caron MG, Lefkowitz RJ. Removal of phosphorylation sites from the beta 2-adrenergic receptor delays onset of agonist-promoted desensitization. Nature. 1988; 333:370–373. [PubMed: 2836733]
15. Krasel C, Zabel U, Lorenz K, Reiner S, Al-Sabah S, Lohse MJ. Dual role of the beta2-adrenergic receptor C terminus for the binding of beta-arrestin and receptor internalization. The Journal of Biological Chemistry. 2008; 283:31840–31848. [PubMed: 18801735]
16. Hausdorff WP, Bouvier M, O'Dowd BF, Irons GP, Caron MG, Lefkowitz RJ. Phosphorylation sites on two domains of the beta 2-adrenergic receptor are involved in distinct pathways of receptor desensitization. The Journal of Biological Chemistry. 1989; 264:12657–12665. [PubMed: 2545714]

17. Kang Y, Zhou XE, Gao X, He Y, Liu W, Ishchenko A, Barty A, White TA, Yefanov O, Han GW, Xu Q, de Waal PW, Ke J, Tan MH, Zhang C, Moeller A, West GM, Pascal BD, Van Eps N, Caro LN, Vishnivetskiy SA, Lee RJ, Suino-Powell KM, Gu X, Pal K, Ma J, Zhi X, Boutet S, Williams GJ, Messerschmidt M, Gati C, Zatsepin NA, Wang D, James D, Basu S, Roy-Chowdhury S, Conrad CE, Coe J, Liu H, Lisova S, Kupitz C, Grotjohann I, Fromme R, Jiang Y, Tan M, Yang H, Li J, Wang M, Zheng Z, Li D, Howe N, Zhao Y, Standfuss J, Diederichs K, Dong Y, Potter CS, Carragher B, Caffrey M, Jiang H, Chapman HN, Spence JC, Fromme P, Weierstall U, Ernst OP, Katritch V, Gurevich VV, Griffin PR, Hubbell WL, Stevens RC, Cherezov V, Melcher K, Xu HE. Crystal structure of rhodopsin bound to arrestin by femtosecond X-ray laser. Nature. 2015; 523:561–567. [PubMed: 26200343]

18. Shukla AK, Manglik A, Kruse AC, Xiao K, Reis RI, Tseng WC, Staus DP, Hilger D, Uysal S, Huang LY, Paduch M, Tripathi-Shukla P, Koide A, Koide S, Weis WI, Kossiakoff AA, Kobilka BK, Lefkowitz RJ. Structure of active β-arrestin-1 bound to a G-protein-coupled receptor phosphopeptide. Nature. 2013; 497:137–141. [PubMed: 23604254]

19. Nobles KN, Xiao K, Ahn S, Shukla AK, Lam CM, Rajagopal S, Strachan RT, Huang TY, Bressler EA, Hara MR, Shenoy SK, Gygi SP, Lefkowitz RJ. Distinct phosphorylation sites on the β(2)-adrenergic receptor establish a barcode that encodes differential functions of β-arrestin. Science Signaling. 2011; 4:ra51. [PubMed: 21868357]

20. Chen YJ, Oldfield S, Butcher AJ, Tobin AB, Saxena K, Gurevich VV, Benovic JL, Henderson G, Kelly E. Identification of phosphorylation sites in the COOH-terminal tail of the μ-opioid receptor. Journal of Neurochemistry. 2013; 124:189–199. [PubMed: 23106126]

21. Howlett AC, Barth F, Bonner TI, Cabral G, Casellas P, Devane WA, Felder CC, Herkenham M, Mackie K, Martin BR, Mechoulam R, Pertwee RG. International union of pharmacology. XXVII. Classification of cannabinoid receptors. Pharmacological Reviews. 2002; 54:161–202. [PubMed: 12037135]

22. Stadel R, Ahn KH, Kendall DA. The cannabinoid type-1 receptor carboxyl-terminus, more than just a tail. Journal of Neurochemistry. 2011; 117:1–18. [PubMed: 21244428]

23. Nie J, Lewis DL. The proximal and distal C-terminal tail domains of the CB1 cannabinoid receptor mediate G protein coupling. Neuroscience. 2001; 107:161–167.

24. Mukhopadhyay S, Cowsik SM, Lynn AM, Welsh WJ, Howlett AC. Regulation of Gi by the CB1 cannabinoid receptor C-terminal juxtamembrane region: structural requirements determined by peptide analysis. Biochemistry. 1999; 38:3447–3455. [PubMed: 10079092]

25. Shim J-Y, Ahn KH, Kendall DA. Molecular basis of cannabinoid CB1 receptor coupling to the G protein heterotrimer Gαiβγ: identification of key CB1 contacts with the C-terminal helix α5 of Gαi. The Journal of Biological Chemistry. 2013; 288:32449–32465. [PubMed: 24092756]

26. Nie J, Lewis DL. Structural domains of the CB1 cannabinoid receptor that contribute to constitutive activity and G-protein sequestration. The Journal of Neuroscience. 2001; 21:8758–8764. [PubMed: 11698587]

27. Jin W, Brown S, Roche JP, Hsieh C, Celver JP, Kovoor A, Chavkin C, Mackie K. Distinct domains of the CB1 cannabinoid receptor mediate desensitization and internalization. The Journal of Neuroscience. 1999; 19:3773–3780. [PubMed: 10234009]

28. Morgan DJ, Davis BJ, Kearn CS, Marcus D, Cook AJ, Wager-Miller J, Straiker A, Myoga MH, Karduck J, Leishman E, Sim-Selley LJ, Czyzyk TA, Bradshaw HB, Selley DE, Mackie K. Mutation of putative GRK phosphorylation sites in the cannabinoid receptor 1 (CB1R) confers resistance to cannabinoid tolerance and hypersensitivity to cannabinoids in mice. The Journal of Neuroscience. 2014; 34:5152–5163. [PubMed: 24719095]

29. Daigle TL, Kearn CS, Mackie K. Rapid CB1 cannabinoid receptor desensitization defines the time course of ERK1/2 MAP kinase signaling. Neuropharmacology. 2008; 54:36–44. [PubMed: 17681354]

30. Teller DC, Okada T, Behnke CA, Palczewski K, Stenkamp RE. Advances in determination of a high-resolution three-dimensional structure of rhodopsin, a model of G-protein-coupled receptors (GPCRs). Biochemistry. 2001; 40:7761–7772. [PubMed: 11425302]

31. Okada T, Sugihara M, Bondar AN, Elstner M, Entel P, Buss V. The retinal conformation and its environment in rhodopsin in light of a new 2.2 A crystal structure. Journal of Molecular Biology. 2004; 342:571–583. [PubMed: 15327956]

32. Murakami M, Kouyama T. Crystallographic analysis of the primary photochemical reaction of squid rhodopsin. Journal of Molecular Biology. 2011; 413:615–627. [PubMed: 21906602]
33. Granier S, Kim S, Shafer AM, Ratnala VR, Fung JJ, Zare RN, Kobilka B. Structure and conformational changes in the C-terminal domain of the beta2-adrenoceptor: insights from fluorescence resonance energy transfer studies. The Journal of Biological Chemistry. 2007; 282:13895–13905. [PubMed: 17347144]
34. Ahn KH, Pellegrini M, Tsomaia N, Yatawara AK, Kendall DA, Mierke DF. Structural analysis of the human cannabinoid receptor one carboxyl-terminus identifies two amphipathic helices. Biopolymers. 2009; 91:565–573. [PubMed: 19274719]
35. Bakshi K, Mercier RW, Pavlopoulos S. Interaction of a fragment of the cannabinoid CB1 receptor C-terminus with arrestin-2. FEBS Letters. 2007; 581:5009–5016. [PubMed: 17910957]
36. Singh SN, Bakshi K, Mercier RW, Makriyannis A, Pavlopoulos S. Binding between a distal C-terminus fragment of cannabinoid receptor 1 and arrestin-2. Biochemistry. 2011; 50:2223–2234. [PubMed: 21306178]
37. Chen C, Okayama H. High-efficiency transformation of mammalian cells by plasmid DNA. Molecular and Cellular Biology. 1987; 7:2745–2752. [PubMed: 3670292]
38. Ahn KH, Bertalovitz AC, Mierke DF, Kendall DA. Dual role of the second extracellular loop of the cannabinoid receptor 1: ligand binding and receptor localization. Molecular Pharmacology. 2009; 76:833–842. [PubMed: 19643997]
39. Bradford MM. A rapid and sensitive method for the quantitation of microgram quantities of protein utilizing the principle of protein-dye binding. Analytical Biochemistry. 2009; 72:248–254.
40. Ahn KH, Mahmoud MM, Kendall DA. Allosteric modulator ORG27569 induces CB1 cannabinoid receptor high affinity agonist binding state, receptor internalization, and Gi protein-independent ERK1/2 kinase activation. The Journal of Biological Chemistry. 2012; 287:12070–12082. [PubMed: 22343625]
41. Mahmoud MM, Ali HI, Ahn KH, Damaraju A, Samala S, Pulipati VK, Kolluru S, Kendall DA, Lu D. Structure activity relationship Study of indole-2-carboxamides identifies a potent allosteric modulator for the cannabinoid receptor 1 (CB1). Journal of Medicinal Chemistry. 2013; 56:7965–7975. [PubMed: 24053617]
42. Bradley P, Misura KM, Baker D. Toward high-resolution de novo structure prediction for small proteins. Science. 2005; 309:1868–1871. [PubMed: 16166519]
43. Misura KM, Chivian D, Rohl CA, Kim DE, Baker D. Physically realistic homology models built with ROSETTA can be more accurate than their templates. Proceedings of the National Academy of Sciences of the United States of America. 2006; 103:5361–5366. [PubMed: 16567638]
44. Rohl CA, Strauss CE, Misura KM, Baker D. Protein structure prediction using Rosetta. Methods in Enzymology. 2004; 383:66–93. [PubMed: 15063647]
45. Dunbrack RL Jr. Karplus M. Backbone-dependent rotamer library for proteins. Application to side-chain prediction. Journal of Molecular Biology. 1993; 230:543–574. [PubMed: 8464064]
46. Pierce BG, Wiehe K, Hwang H, Kim BH, Vreven T, Weng Z. ZDOCK server: interactive docking prediction of protein-protein complexes and symmetric multimers. Bioinformatics. 2014; 30:1771–1773. [PubMed: 24532726]
47. Humphrey W, Dalke A, Schulten K. VMD - Visual Molecular Dynamics. J. Mol. Graph. 1996; 14.1:33–38. [PubMed: 8744570]
48. Phillips JC, Braun R, Wang W, Gumbart J, Tajkhorshid E, Villa E, Chipot C, Skeel RD, Kalé L, Schulten K. Scalable molecular dynamics with NAMD. Journal of Computational Chemistry. 2005; 26:1781–1802. [PubMed: 16222654]
49. Brooks BR, Brooks CL III, Mackerell AD, Nilsson L, Petrella RJ, Roux B, Won Y, Archontis G, Bartels C, Boresch S, Caflisch A, Caves L, Cui Q, Dinner AR, Feig M, Fischer S, Gao J, Hodoscek M, Im W, Kuczera K, Lazaridis T, Ma J, Ovchinnikov V, Paci E, Pastor RW, Post CB, Pu JZ, Schaefer M, Tidor B, Venable RM, Woodcock HL, Wu X, Yang W, York DM, Karplus M. CHARMM: The Biomolecular simulation Program. Journal of Computational Chemistry. 2009; 30:1545–1615. [PubMed: 19444816]
50. Best RB, Zhu X, Shim J, Lopes PE, Mittal J, Feig M, Mackerell AD Jr. Optimization of the additive CHARMM all-atom protein force field targeting improved sampling of the backbone $\phi$, $\psi$

and side-chain χ(1) and χ(2) dihedral angles. Journal of Chemical Theory and Computation. 2012; 8:3257–3273. [PubMed: 23341755]

51. Klauda JB, Venable RM, Freites JA, O'Connor JW, Tobias DJ, Mondragon-Ramirez C, Vorobyov I, MacKerell AD Jr, Pastor RW. Update of the CHARMM all-atom additive force field for lipids: validation on six lipid types. The Journal of Physical Chemistry B. 2010; 114:7830–7843. [PubMed: 20496934]
52. Jorgensen WL, Chandrasekhar J, Madura JD, Impey RW, Klein ML. Comparison of Simple Potential Functions for Simulating Liquid Water. The Journal of Chemical Physics. 1983; 79:926–935.
53. Feller SE, Zhang Y, Pastor RW, Brooks BR. Constant pressure molecular dynamics simulation: the Langevin piston method. The Journal of Chemical Physics. 1995; 103:4613–4621.
54. Hoover WG. Canonical dynamics: Equilibrium phase-space distributions. Phys. Rev. 1985; A31:1695–1697.
55. Essmann U, Perera L, Berkowitz ML, Darden T, Lee H, Pedersen LG. A smooth particle mesh Ewald method. The Journal of Chemical Physics. 1995; 103:8577–8593.
56. Tuckerman M, Berne BJ. Reversible multiple time scale molecular dynamics. The Journal of Chemical Physics. 1992; 97:1990–2001.
57. Laskowski RA, MacArthur MW, Moss DS, Thornton JM. PROCHECK - a program to check the stereochemical quality of protein structures. Journal of Applied Crystallography. 1993; 26:283–291.
58. Ahn KH, Scott CE, Abrol R, Goddard WA, Kendall DA. Computationally-predicted CB1 cannabinoid receptor mutants show distinct patterns of salt-bridges that correlate with their level of constitutive activity reflected in G protein coupling levels, thermal stability, and ligand binding. Proteins. 2013; 81:1304–1317. [PubMed: 23408552]
59. Grossfield A, Feller SE, Pitman MC. Convergence of molecular dynamics simulations of membrane proteins. Proteins. 2007; 67:31–40. [PubMed: 17243153]
60. Sugita Y, Okamoto Y. Replica-exchange molecular dynamics method for protein folding. Chemical Physics Letters. 1999; 314:141–151.
61. García AE, Sanbonmatsu KY. Alpha-helical stabilization by side chain shielding of backbone hydrogen bonds. Proceedings of the National Academy of Sciences of the United States of America. 2002; 99:2782–2787. [PubMed: 11867710]
62. Day R, Paschek D, Garcia AE. Microsecond simulations of the folding/unfolding thermodynamics of the Trp-cage miniprotein. Proteins. 2010; 78:1889–1899. [PubMed: 20408169]
63. Czaplewski C, Kalinowski S, Liwo A, Scheraga HA. Application of Multiplexed Replica Exchange Molecular Dynamics to the UNRES Force Field: Tests with alpha and alpha+beta Proteins. Journal of Chemical Theory and Computation. 2009; 5:627–640. [PubMed: 20161452]
64. Kaufmann KW, Lemmon GH, Deluca SL, Sheehan JH, Meiler J. Practically useful: what the Rosetta protein modeling suite can do for you. Biochemistry. 2010; 49:2987–2998. [PubMed: 20235548]
65. Vreven T, Pierce BG, Hwang H, Weng Z. Performance of ZDOCK in CAPRI rounds 20-26. Proteins. 2013; 81:2175–2182. [PubMed: 24123140]
66. Rost B, Yachdav G, Liu J. The PredictProtein server. Nucleic Acids Research. 2004; 32:321–326.
67. Dolinsky TJ, Nielsen JE, McCammon JA, Baker NA. PDB2PQR: an automated pipeline for the setup, execution, and analysis of Poisson-Boltzmann electrostatics calculations. Nucleic Acids Research. 2004; 32:W665–W667. [PubMed: 15215472]

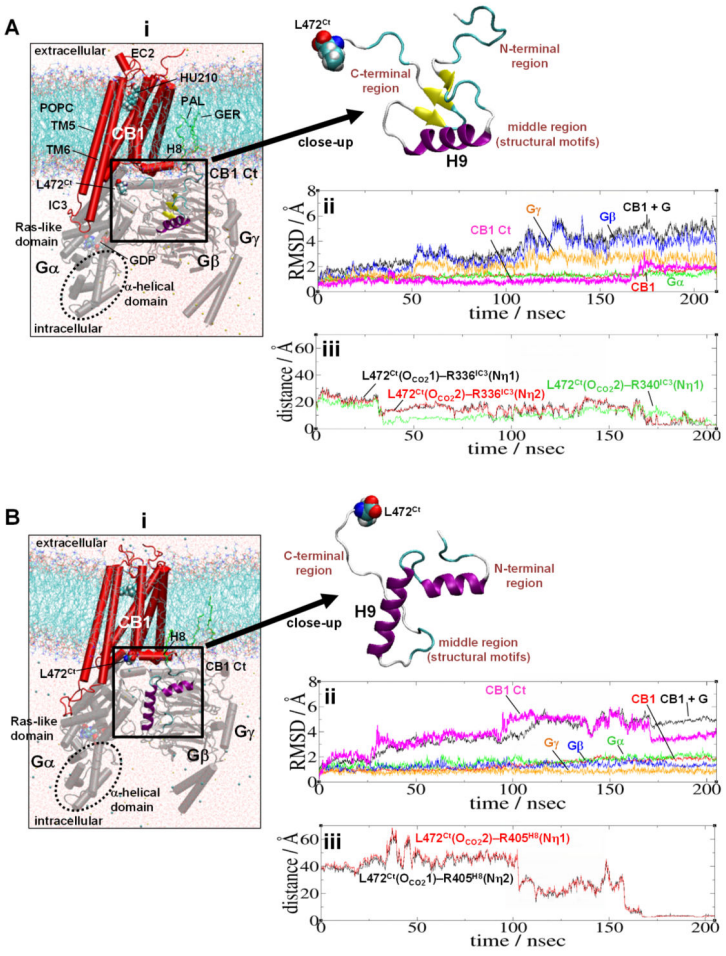


**Figure 1. Two simulation systems of the CB1-Gi complex, CB1($A^{Ct}$)-Gi (A) and CB1($B^{Ct}$)-Gi (B), at the end of 205 ns simulations**

(i) The CB1 receptor is represented in red cartoon, while Gi is represented in grey cartoon. CB1 Ct with the structural motifs (α-helix, purple; β-sheet, yellow; turn, cyan; and coil, white) in the middle region are indicated by a box. PALs, which are covalently bonded to $Cys415^{H8}$ of the CB1 receptor and $Cys3^{G\alpha i}$, and GER, which is covalently bonded to $Cys68^{G\gamma}$, are represented by green sticks. The CB1 agonist HU210 bound to the receptor, GDP bound to Gα, and the CB1 Ct extreme end residue $Leu472^{Ct}$ are represented by space-filling (atom-type). Lipids and water molecules are represented as lines (atom-type), while ions ($Na^+$ in cyan and $Cl^-$ in yellow) are represented as balls. The α-helical domain of Gα, whose movements are crucial for G protein activation, is indicated by a dotted circle. Lipid and water hydrogen atoms are omitted for clarity. Color coding for atoms: C, cyan; N, blue; O, red; and S, yellow. (ii) RMSD values of the CB1-Gi complex, for the whole complex (in black), for the CB1 receptor (in red), for Gα (in green), for Gβ (in blue), for Gγ (in orange), and CB1 Ct (in magenta), calculated by RMS fitting of the coordinates taken during the simulation to the initial coordinates, with respect to the backbone $C_\alpha$ atoms of secondary structure. (iii) Strong attractions between the CB1-Gα/Gβ interfacial region and the Ct end residue $Leu472^{Ct}$ in CB1($\mathbf{A^{Ct}}$)-Gi, measured by side chain distances of $Leu472^{Ct}(O_{CO2}1)$–$Arg336^{Ct}(N\eta1)$ (black), $Leu472^{Ct}(O_{CO2}2)$–$Arg336^{Ct}(N\eta2)$ (red), and $Leu472^{Ct}(O_{CO2}2)$–

Arg340$^{Ct}$(Nη1) (green) and in CB1(**B$^{Ct}$**)-Gi, measured by side chain distances of Leu472$^{Ct}$($O_{CO2}$1)–Arg405$^{Ct}$(Nη2) (black) and Leu472$^{Ct}$($O_{CO2}$2)–Arg405$^{Ct}$(Nη1) (red).

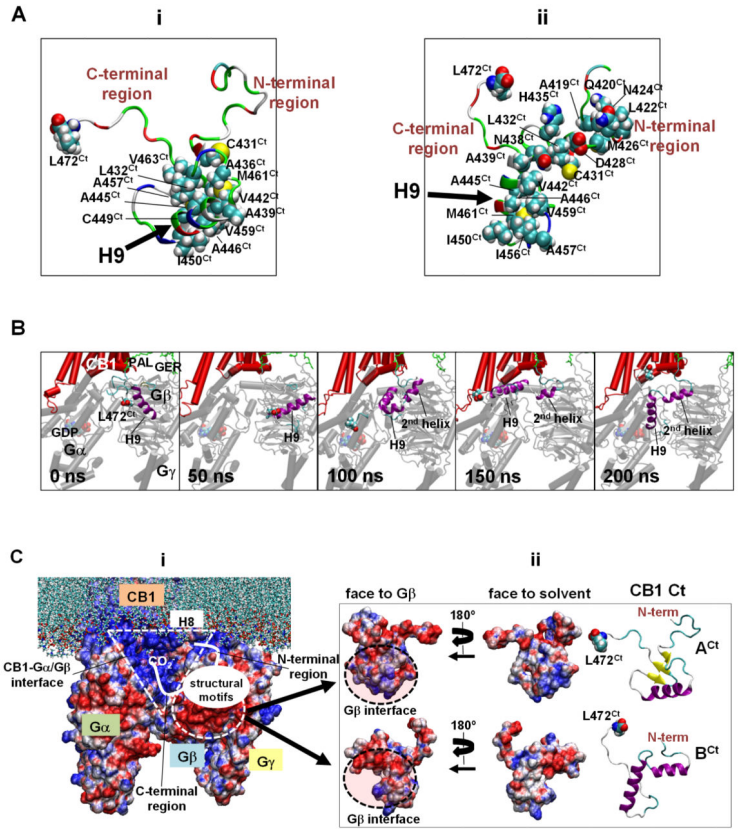


**Figure 2. Molecular features of the CB1 Ct**

**A**. Hydrophobic clusters centered at H9 in (i) $\mathbf{A}^{\mathbf{Ct}}$ in CB1($\mathbf{A}^{\mathbf{Ct}}$)-Gi and (ii) $\mathbf{B}^{\mathbf{Ct}}$ in CB1($\mathbf{B}^{\mathbf{Ct}}$)-Gi. Hydrophobic residues forming the clusters along with the extreme C-terminal end residue Leu472$^{Ct}$ are represented by space-filling (atom-type). **B**. The development of the second helix in the N-terminal region of $\mathbf{B}^{\mathbf{Ct}}$ in CB1($\mathbf{B}^{\mathbf{Ct}}$)-Gi examined by snapshots taken at different times of the simulation: 0 ns, 50 ns, 100 ns, 150 ns, and 200 ns. **C.** The Poisson–Boltzmann electrostatic potential map of the CB1-Gi complex, calculated using the APBS web server[67]. (i) The surface of the CB1-Gi complex is rendered in blue and red to illustrate electrostatically positive and negative regions, respectively, in the APBS potential data ranging from +4 to −4. (ii) The surfaces of $\mathbf{A}^{\mathbf{Ct}}$ in CB1($\mathbf{A}^{\mathbf{Ct}}$)-Gi and $\mathbf{B}^{\mathbf{Ct}}$ in CB1($\mathbf{B}^{\mathbf{Ct}}$)-Gi in the middle are rendered in blue and red to illustrate electrostatically positive and negative regions, respectively, in the APBS potential data ranging from +4 to −4. The surface of the CB1 Ct interface to Gβ on the right was obtained by rotating the CB1 Ct 180° about the z axis. The dotted circles indicate the region of Gβ where the electrostatic potential surface is highly negative.

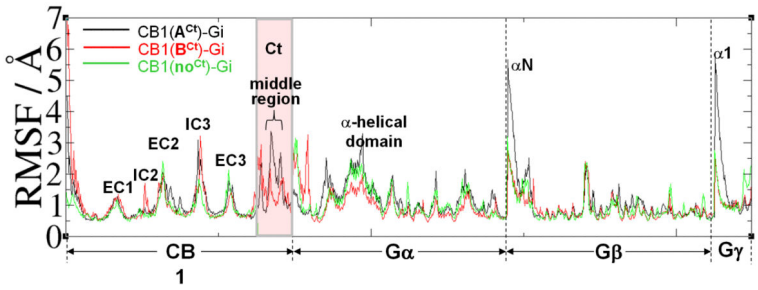


**Figure 3. Inherent flexibility in the CB1 Ct**

RMSF plots of CB1(**A**$^{\mathbf{Ct}}$)-Gi (in black), CB1(**B**$^{\mathbf{Ct}}$)-Gi (in red), and CB1(**no**$^{\mathbf{Ct}}$)-Gi[24] (in green), obtained by calculating the variance of every atom position over the trajectories of the last 20 ns of the simulation. CB1 Ct is square-marked in red.

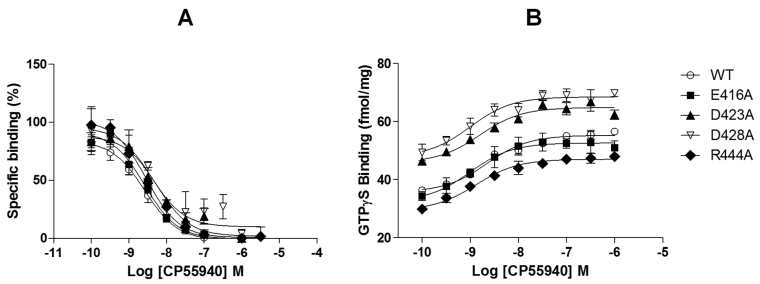


**Figure 4. Site-directed mutagenesis studies of CB1 Ct in the CB1-Gi complex**

**A**. Competition binding of the agonist CP55,940 using [$^{3}$H]CP55,940 as tracer. Non-specific binding was determined in the presence of 1 μM unlabeled CP55,940 for competition binding. **B**. CP55,940-induced [$^{35}$S]GTPγS to assess G protein coupling. 10 μM unlabeled GTPγS was used. In all cases, cell membranes expressing the wild-type CB1 receptor (o), Glu416$^{Ct}$Ala (■), Asp423$^{Ct}$Ala (▲), Asp428$^{Ct}$Ala (▽) or R444$^{Ct}$Ala (◆) mutated receptors were evaluated. Data points represent the mean ± S.E. (error bars) of at least three independent experiments performed in duplicate.

## Table 1

The secondary structure analysis for the CB1 Ct (Glu416$^{Ct}$-Leu472$^{Ct}$) in the two distinct models **A$^{Ct}$** in CB1(**A$^{Ct}$**)-Gi and **B$^{Ct}$** in CB1(**B$^{Ct}$**)-Gi, in comparison with the NMR-predicted structures of the CB1 Ct peptides. The residues used in the present site-directed mutagenesis studies are indicated in bold. The segment that showed a close correlation with the α-helical domain of Gα in CB1(**A$^{Ct}$**)-Gi are shaded. One-letter coding for secondary structure: E, β-sheet; and H, α-helix. For the NMR structures, a phosphorylation-free peptide in DPC[34], the Ser425$^{Ct}$ and Ser429$^{Ct}$ di-phosphorylated peptide in complex with β-arrestin-1[35] and Thr460$^{Ct}$, Ser462$^{Ct}$, Ser464$^{Ct}$, Thr467$^{Ct}$, and Ser468$^{Ct}$ multi-phosphorylated peptide in complex with β-arrestin-1[36] were used. For the prediction, PredictProtein[66] was used.

| | Secondary structure |
|---|---|
| | 416 472<br>**E**GTAQPL**D**NSMG**D**SDCLHKHANNAASVH**R**AAESCIKSTVKIAKVTMSVSTDTSAEAL |
| NMR structure<br>Ref. 34<br>Ref. 35<br>Ref. 36 | ----------HHHHHHHHHHHHHHHHHHHHH----------<br>----HHHHH-HHHHH-----<br>----------HHHHH-- |
| Predicted structure | ----------HHHHHHHH---HHHHHHHHHHHHHHHHHHHEEEE---HHH--- |
| **A$^{Ct}$**<br>**B$^{Ct}$** | ----------EE-------HHHHHHHHHHHH-----EE---EE---------<br>-------HHHHHHHHH-----HHHHHHHHHHHHHH----------- |

## Table 2

Intra- and inter-molecular interactions of CB1 Ct in the two distinct models $\mathbf{A^{Ct}}$ in CB1($\mathbf{A^{Ct}}$)-Gi and $\mathbf{B^{Ct}}$ in CB1($\mathbf{B^{Ct}}$)-Gi. Hydrophobic interactions involved by polar/charged residues occur through their aliphatic hydrocarbon portions, while H-bonding and salt bridge interactions involved by nonpolar residues occur through their backbone amides or the terminal carboxylates.

| Model | Intra-molecular (within CB1) | | Inter-molecular (with G protein) | |
|---|---|---|---|---|
| | Carboxyl-terminus | IC3 and H8 | Gα | Gβ |
| **$A^{Ct}$**<br>*H9:*<br>$A439^{Ct}$–$K451^{Ct}$<br>*β-bridge:*<br>$D430^{Ct}$–$C431^{Ct}$<br>$A457^{Ct}$–$K458^{Ct}$<br>$S462^{Ct}$–$V463^{Ct}$ | *hydrophobic cluster*:<br>$C431^{Ct}$/$L432^{Ct}$/<br>$A436^{Ct}$/$A439^{Ct}$/<br>$V442^{Ct}$/$A445^{Ct}$/<br>$A446^{Ct}$/$C449^{Ct}$/<br>$I450^{Ct}$/$A457^{Ct}$/<br>$V459^{Ct}$/$M461^{Ct}$/<br>$V463^{Ct}$<br>*salt bridge:*<br>$R444^{Ct}$–$E447^{Ct}$ | *H-bonding and salt bridge:*<br>$L472^{Ct}$–$R336^{IC3}$<br>$L472^{Ct}$–$R340^{IC3}$<br>$E416^{Ct}$–$R409^{H8}$<br>$D428^{Ct}$–$R409^{H8}$<br>$S468^{Ct}$–$K402^{H8}$ | *hydrophobic:*<br>$V454^{Ct}$/$K455^{Ct}$–<br>$K257^{Gα}$<br>$L472^{Ct}$–$T316^{Gα}$<br>*salt bridge:*<br>$E470^{Ct}$–$K257^{Gα}$ | *hydrophobic:*<br>$S425^{Ct}$/$M426^{Ct}$–<br>$V307^{Gβ}$/$A309^{Gβ}$<br>$I456^{Ct}$/$S429^{Ct}$/<br>$S462^{Ct}$/$S464^{Ct}$–<br>$I270^{Gβ}$<br>*salt bridge:*<br>$D423^{Ct}$–$R42^{Gβ}$<br>$K458^{Ct}$–$D246^{Gβ}$<br>$K458^{Ct}$–$D247^{Gβ}$ |
| **$B^{Ct}$**<br>*2nd helix:*<br>$D423^{Ct}$–$L432^{Ct}$<br>*H9:*<br>$N437^{Ct}$–$S452^{Ct}$ | *hydrophobic cluster1:*<br>$N420^{Ct}$/$P421^{Ct}$/<br>$L422^{Ct}$/$N424^{Ct}$/<br>$S425^{Ct}$/<br>*hydrophobic cluster2:*<br>$A439^{Ct}$/$V442^{Ct}$/<br>$A445^{Ct}$/$A446^{Ct}$/<br>$C449^{Ct}$/$I450^{Ct}$/<br>$V459^{Ct}$/$I456^{Ct}$/<br>$V459^{Ct}$/$M461^{Ct}$<br>*H-bonding and salt bridge:*<br>$E416^{Ct}$–$T418^{Ct}$<br>$R444^{Ct}$–$D466^{Ct}$ | *hydrophobic:*<br>$A471^{Ct}$–$R340^{IC3}$<br>$E416^{Ct}$–$R409^{H8}$<br>$E416^{Ct}$–$C415^{H8}$<br>*salt bridge:*<br>$E416^{Ct}$–$R409^{H8}$<br>$L472^{Ct}$–$R405^{H8}$ | *hydrophobic:*<br>$T467^{Ct}$/$A469^{Ct}$–<br>$T316^{Gα}$/$K317^{Gα}$<br>*H-bonding and salt bridge:*<br>$K451^{Ct}$–$D251^{Gα}$<br>$D466^{Ct}$–$K257^{Gα}$<br>$T467^{Ct}$–$D261^{Gα}$<br>$T467^{Ct}$–$K317^{Gα}$ | *hydrophobic:*<br>$A419^{Ct}$/$M426^{Ct}$–<br>$V307^{Gβ}$/$A309^{Gβ}$<br>$C431^{Ct}$/$V459^{Ct}$–<br>$I270^{Gβ}$<br>*salt bridge:*<br>$D423^{Ct}$–$R42^{Gβ}$<br>$D423^{Ct}$–$R304^{Gβ}$<br>$D430^{Ct}$–$R314^{Gβ}$ |

## Table 3

Ligand binding and G protein coupling parameters for the wild-type CB1 receptor and the mutant receptors. Data are presented as the mean ± S.E. for the $K_i$ values, basal levels and CP55,940-induced $E_{max}$ values and the median and corresponding 95% confidence limits for the $EC_{50}$ values, from at least three independent assays performed in duplicate.

| | CP55,940 Binding | GTPγS Binding | | |
|---|---|---|---|---|
| | | Basal Levels | CP55,940-induced | |
| | $K_i$ (nM) | (fmol/mg) | $EC_{50}$ (nM) | $E_{max}$ (fmol/mg) |
| Wild type | 1.8 ± 1.2 | 38.1 ± 0.6 | 2.2 ± (1.4-3.5) | 55.3 ± 0.5 |
| $Glu416^{Ct}Ala$ | 1.9 ± 1.2 | 35.7 ± 1.5 | 1.0 (0.3-3.0) | 52.6 ± 1.1 |
| $Asp423^{Ct}Ala$ | 3.6 ± 1.3 | 45.9 ± 1.3* | 1.6 (0.8-3.1) | 64.8 ± 0.7*** |
| $Asp428^{Ct}Ala$ | 2.5 ± 1.7 | 53.6 ± 2.7*** | 1.0 (0.3-2.9) | 68.5 ± 1.1*** |
| $Arg444^{Ct}Ala$ | 1.6 ± 1.2 | 31.7 ± 0.4 | 1.3 (0.7-2.4) | 47.0 ± 0.6*** |

Asterisks depict the statistically significant differences in the GTPγS assay parameters compared to the wild-type CB1 receptor using analysis of variance followed by Bonferroni's post hoc test:

*, $p < 0.05$,

**, $p < 0.01$,

***, $p < 0.001$. No statistically significant differences were observed in $K_i$ and $EC_{50}$ values of any of the tested receptors from the wild-type CB1 receptor.